CSCP: Energy Charging Mechanism for Surveillance Quality, Network Connectivity and Perpetual Lifetime in WRSNs

Yuanping Kan[1], Chih-Yung Chang[2], Shih-Jung Wu[2], Chin-Hwa Kuo[2], Diptendu Sinha Roy[3]*

[1] Fujian Polytechnic Normal University, China
[2] Tamkang University, Taiwan
[3] National Institute of Technology, India
done0250@126.com, cychang@mail.tku.edu.tw, wushihjung@mail.tku.edu.tw,
chinhwakuo@mail.tku.edu.tw, diptendu.sr@nitm.ac.in

Abstract

In recent years, wireless charging techniques applied to sensor networks have been widely studied. The sensors in most studies are considered to be equally important, and the main purpose is to maintain the working sensors as many as possible. However, different sensors have different contributions to the surveillance application, especially for network connectivity and surveillance quality. The sensor closer to the base station has a larger contribution to network connectivity since its failure can block more data transmissions. On the other hand, a sensor in a sparse area has a larger contribution to surveillance quality because few or no neighboring sensors can execute the sensing operation instead of the sensor if it is energy exhaustion. This paper proposes an energy recharging mechanism, called *CSCP*, which adopts the mobile charger to recharge the sensors according to the recharging requests. The proposed *CSCP* considers the contribution of each grid in terms of network connectivity, surveillance quality as well as path cost, aiming to recharge the grids where the sensors can maximize the surveillance quality. Performance research reveals that the proposed *CSCP* has better performance than the related studies in the surveillance quality, the number of working sensors, and recharging efficiency.

Keywords: Wireless rechargeable sensor networks, Surveillance quality, Connectivity, Recharging, Mobile charger

1 Introduction

Wireless rechargeable sensor network (WRSN) has become an important network in recent years due to its wide applications, such as military surveillance, health monitoring, industrial automation, smart city, natural disaster relief, etc. [1-2]. The WRSN usually consists of many small sensors powered by rechargeable batteries. Since each sensor is small, the capacity of its battery is limited. As a result, the lifetime of WRSN usually obstructs the large-scale deployment of WRSN. In recent years, extensive efforts have been made to recharge the sensors, aiming to achieve the perpetual lifetime of WRSN. The recharging mechanisms can be classified into energy harvesting [3-6] and wireless energy transfer [7-10]. In the class of energy harvesting, the energy obtained from external sources such as solar power, thermal energy, and wind energy is unstable, resulting in the instability of the WRSN. Therefore, it is an urgent problem to find a stable power supply for the sensors.

As a revolutionary energy supply technology, the advent of wireless energy transfer technologies [7-10] provides another option to achieve the perpetual lifetime of the WRSN. Compared to energy harvesting, wireless energy transfer technology can wirelessly transmit energy with a stable and high charging rate, which is a promising technology. Therefore, when the sensors are located within the limited charging range of the mobile charger, they can be recharged. Since most studies assumed that the sensors are static, the recharging task is usually performed by a mobile charger, which receives the recharging requests from the sensors and moves to recharge them.

In literature, many recharging algorithms were proposed to charge the sensors in WRSN. According to the recharging request messages, the mobile charger determined the recharging stations and constructed the recharging path. These studies can be further divided into two categories: the flatten-based category [11-13] and the grid-based category [14-16]. In the flatten-based category, the mobile charger moved to the requested sensors and timely recharged them. Most of these algorithms aimed to recharge more sensors. Therefore their main consideration is the path length cost of the recharging task. On the other hand, in the grid-based category, studies [14-16] divided the monitoring area of WRSN into grids to simplify the problem and scheduled the recharging locations. Then they constructed the recharging path accordingly. However, all the sensors were considered to be equally important for surveillance quality.

This paper aims to maintain the maximum surveillance quality of the monitoring area by developing a recharging mechanism that considers the importance of monitoring quality, network connectivity, and the perpetual lifetime of the sensors. This paper proposes a recharging mechanism, called *CSCP*, which initially divides the monitoring area into several regular hexagon grids. Then it makes a recharging schedule on demand for the grids where the sensors have small remaining energy. To maximize the surveillance quality, it evaluates the recharging weights of the grids based

*Corresponding Author: Chin-Hwa Kuo; E-mail: chinhwakuo@mail.tku.edu.tw
DOI: 10.53106/160792642023032402023

on the surveillance quality, network connection as well as recharging cost. The grid with the maximum weight will be selected to be recharged. Then an efficient path to recharging the sensors in this grid will be constructed.

The main contributions of this work are listed as follows.

(1) Surveillance Quality Awareness.

Most of the existing charging mechanisms took into account the length of the charging path and the number of charged sensors. However, they did not consider that surveillance quality is the most important purpose of sensor networks. In contrast to existing studies [11, 15], the proposed *CSCP* algorithm further takes into account the factors that might impact the surveillance quality of each sensor. The sensors with a larger contribution to the surveillance quality will be earlier to be recharged. Therefore, the proposed *CSCP* algorithm can obtain better surveillance quality as compared with the related studies [11] and [15].

(2) Connectivity Awareness.

When the network is disconnected, the sensing data will not be delivered to the base station even if many sensors are working on sensing data. Therefore connectivity plays an important role in evaluating the importance of the sensors. The proposed *CSCP* algorithm further takes into account the connectivity contribution of each sensor. The sensors with a larger connectivity contribution will be earlier to be recharged. Compared with the related studies [11, 15], the *CSCP* achieves better network connection. Therefore, more data are collected by the base station.

(3) Recharging While Moving Along an Efficient Path.

In this work, the target area is firstly divided into several regular hexagonal grids. When the mobile charger determines to recharge one grid, the mobile charger will further construct an efficient path along which the mobile charger can move and recharge the sensors in the target grid. Herein, it is noticed that the charger can wirelessly recharge the sensors if the distance between the sensors and the mobile charger is smaller than the charging radius. To ensure that each sensor can be fully recharged, the Full Recharged Range property, denoted by FR^2, is proposed, which ensures that each sensor is fully recharged by the mobile charger.

The following describes the organization of the remaining part of this paper. Section II reviews the existing work. Section III states the problem investigated in this paper and the assumptions. Section IV details the proposed *CSCP* mechanism. Section V further compares the performance of the proposed *CSCP* algorithm against the related studies. Finally, a conclusion of the proposed algorithm and future work are presented.

2 Related Work

In the literature, previous studies on developing recharging mechanisms using a mobile charger can be mainly divided into two categories: the flatten-based category and the grid-based category.

2.1 The Flatten-based Model

Some existing studies fall into the flatten-based category. Yu et al. [11] extended the lifetime of the WRSN using a mobile charger. When the remaining energy of a sensor was less than a predetermined threshold, a recharging request of the sensor will be transmitted to the mobile charger. Upon receiving the requests, it firstly built an initial charging path crossing all the requested sensors. Then, the length of the charging path was reduced using a path reduction algorithm.

Xu et al. [12] divided the sensors into different groups according to the charging radius of the mobile charger. Therefore, it can charge the sensors in each group simultaneously. Then it constructed a closed recharging path for reducing the recharging delay.

Sha et al. [13] divided the sensors into clusters based on their remaining energy. It aimed to timely recharge the low-energy sensors. In addition, it aimed to balance the workloads of all mobile chargers. To achieve this goal, it further considered the path length and the energy consumption of all mobile chargers. In summary, the aforementioned studies [11-13] attempted to shorten the path length of the charger. However, they did not take into account the surveillance quality and network connectivity parameters.

2.2 The Grid-based Model

In this grid-based class, the target area is firstly partitioned into several equally sized grids. Then the header of each grid will calculate the recharging needs. Therefore, the mobile charger can construct the recharging path according to the requests of the grids.

Dande et al. [14] divided the target area into some equal-sized grids. The sensors, which fall within the charging coverage of a grid and remained low energy, will be treated as a charging candidate set. The mobile charger should move to the grid center for recharging the sensors in that grid. According to the coverage contribution of the candidate set and the cost of the recharging path, the mobile charge made a schedule and constructed a path for that schedule.

Kan et al. [15] also divided the surveillance area into several cells. The mobile charger evaluated the coverage contribution for each grid. The grid with the maximum coverage contribution was preferentially recharged by the mobile charger.

Yang et al. [16] divided the monitoring area into several layers of square rings. The mobile charger was initially located at the center of the whole region. It firstly made a recharging schedule in the three inner square rings by using the Nearest Neighbor method. Then it moved along the edge of the outer rings and recharge the sensors in the outer rings. The time required for recharging in each square ring can be estimated according to the energy consumption rates. It guaranteed that every sensor can obtain its energy before its remaining energy is smaller than a predefined threshold.

Nevertheless, most of the existing studies fall into the grid-based category and only took into account the number of low-energy sensors in each grid. In contrast to them, this paper further considers the contributions of the surveillance quality and network connectivity of each sensor. Table 1 concludes the contrasts between the related studies and the proposed *CSCP*.

Table 1. Comparison between algorithms

	Grid-based networks	Online scheduling	Considering surveillance quality	Considering connectivity
YCC [11]	×	×	×	×
XLJKXZ [12]	×	×	×	×
SSM [13]	×	×	×	×
DCKYR [14]	○	×	×	×
KCKR [15]	○	○	×	○
YHLQZ [16]	○	×	×	×
CSCP	○	○	○	○

○ = considered, × = not considered

3 Assumptions and Problem Statement

Section III first presents the network environment and assumptions of this paper. After that, the problem statement of this study is described.

3.1 Network Environment

A wireless rechargeable sensor network (WRSN) consists of n_M static sensors $S = \{ S_1, S_2, ..., S_{n_M} \}$ which are randomly deployed in a square monitoring area M with a length L_M. There is a sink node BS located at the center location of M, aiming to collect the sensing data from sensors using multi-hop transmissions. Each sensor is powered by a limited-capacity battery with a wireless recharging device. There are two mobile chargers, denoted by MC_{work} and $MC_{standby}$. For simplicity, the following uses MC to denote the MC_{work}. The MC moves with a constant speed v and charges sensors according to its schedule. On the other hand, the $MC_{standby}$ is recharged at the BS and is on standby waiting to take over the recharging task when the MC moves back to the BS. Then the first charging cycle of the recharging task is finished and another recharge cycle starts. In the new cycle, the two mobile chargers will exchange their roles.

Let T denote the charging cycle which is the duration starting from the MC leaves BS, moves and charges some sensors, and finally returns to BS. Let notation r_s represent the sensing range and notation r_c represent the communication range of each sensor. Assume that the BS can collect the location of each sensor at the network initialization. Furthermore, it is assumed that the mobile charger is aware of its own and each sensor's locations. Let $d_{i,j}$ denote the Euclidean distance between the sensors s_i and s_j. Let $d_{i,MC}$ denote the Euclidean distance between the sensor s_i and the MC. The energy model presented in this paper is described below.

3.2 Energy Model

Let E denote the battery capacity of each sensor. Let E_i^{min} denote the energy threshold at which the sensor will transfer to the sleep state. Let $E_i^{request}$ denote the request threshold of energy at which the sensor s_i will send the recharging request to the BS. The BS will maintain the location of MC and forward the received new requests to MC.

Assume that k denotes the length of the data packet which contains both control information and sensing data. Let e_s denote the energy dissipation for sensing. Let e_R and e_T represent the energy dissipations for receiving and sending each packet (k bits), respectively. The value of e_R can be calculated by $e_R = k \times e_p$, where e_p denotes the energy dissipation per bit incurred by the electronic circuit. The e_T can be calculated by $e_T = k \times \left(e_p + d_{i,j}^2 \times e_f \right)$, where e_f denotes the energy dissipation per bit by the amplifier in free space [17].

Let Φ be the network observing time during which the surveillance quality will be measured. Let $E_{i,t}^{rem}$ denote the residual energy of the sensor s_i at time $t \in \Phi$. Let Boolean variable $\lambda_{i,t}$ denote the state of the sensor s_i at time t. The value of $\lambda_{i,t}$ can be obtained by applying Exp. (1).

$$\lambda_{i,t} = \begin{cases} 1 & E_{i,t}^{rem} > E_i^{min} \\ 0 & otherwise \end{cases}. \tag{1}$$

Let notation $\beta_{i,t}$ be a Boolean variable that represents whether or not the sensor s_i and BS is connected at time t. That is,

$$\beta_{i,t} = \begin{cases} 1 & s_i \ and \ BS \ is \ connected \\ 0 & otherwise \end{cases}. \tag{2}$$

Let R_{s_i} denote the spatial representation of the sensor s_i. The surveillance quality of WRSN at time t can be measured by applying Eq. (3).

$$Q_{net}^t = \bigcup_{s_i \in S} \lambda_{i,t} \times \beta_{i,t} \times R_i. \tag{3}$$

Let E_{i,t_j}^c denote the recharged energy from the MC to the sensor s_i at time t_j. Let E_{i,t_j}^s, E_{i,t_j}^R and E_{i,t_j}^T represent the energy dissipation of the sensor s_i to execute the sensing, data receiving, and data transmission operations at the time t_j, respectively. Let $\rho_{i,t}^{sensing}$, $\rho_{i,t}^{receiving}$ and $\rho_{i,t}^{transmit}$ be Boolean variables which represent whether or not sensor s_i executes sensing, data receiving, and data transmission, respectively, at time t.

Let notation γ_{i,t_j} denote a Boolean variable representing whether or not s_i is charged at the time t_j. That is,

$$\gamma_{i,t_j} = \begin{cases} 1 & s_i \ is \ charged \ at \ time \ t_j \\ 0 & otherwise \end{cases}. \tag{4}$$

Then the value of $E_{i,t}^{rem}$ can be calculated by Eq. (5):

$$E_{i,t}^{rem} = E - \sum_{t_j=t_0}^{t} \left(\begin{pmatrix} \rho_{i,t_j}^{sensing} \times E_{i,t_j}^{s} + \\ \rho_{i,t_j}^{receiving} \times E_{i,t_j}^{R} + \\ \rho_{i,t_j}^{transmit} \times E_{i,t_j}^{T} \end{pmatrix} \times \lambda_{i,t_j} - \gamma_{i,t_j} \times E_{i,t_j}^{c} \right). \quad (5)$$

Based on the aforementioned energy model, the goal of this study is given below.

3.3 Objective

This paper aims to obtain the maximum surveillance quality of the monitoring area. The objective can be carried out by obtaining the maximal surveillance quality at any time. Exp. (6) shows the goal of this study.

***Objective*:**

Given an observation period Φ, the minimal surveillance quality of any time $t \in \Phi$ can be maximized. That is,

$$\boldsymbol{max}\left(\min_{t \in \Phi} Q_{net}^{t} \right). \quad (6)$$

3.4 Constraints

Some constraints should be satiated. The first constraint is the *Recharged Energy Bound Constraint* which constrains the maximum recharged energy of each sensor. The following further explains the details of this constraint.

Let P_{MC} and P_{s_i} represent the transmitted and recharged energies of the MC and sensor s_i, respectively. Based on the energy charging model presented in [18], the received energy P_{s_i} of the sensor s_i can be derived as shown in Eq. (7).

$$P_{s_i} = P_{MC} \times f_{i,MC} / (d_{i,MC} + f_F)^2, \quad (7)$$

where $f_{i,MC}$ denotes the transmission factor and fF denotes the parameter to adjust the Friis free-space equation for short-distance transmission. Let r_{MC} denote the charging radius of the MC. To be recharged, the distance of the sensor s_i and *MC* should be smaller than the charging radius of the *MC*. That is, r_{MC} should be greater. Hence, the lower bound of the P_{s_i} is

$$P_{MC} \times f_{i,MC} / (r_{MC} + f_F)^2. \quad (8)$$

Since the recharged energy of s_i comes from the *MC*, the transmitted power of the MC must be greater than the recharged power of the sensor s_i, which is the upper bound. Putting Eqs. (7) and (8) together, the minimal and maximal received energies of each sensor s_i can be obtained by the following recharged energy constraint.

(1) *Recharged Energy Bound Constraint*

$$P_{MC} \times f_{i,MC} / (r_{MC} + f_F)^2 \le P_{s_i} \le P_{MC}. \quad (9)$$

In addition to this constraint, the sensor also needs to have minimal energy for basic action and state transfer. To guarantee enough remaining energy for these basic operations, the sensor can send a request earlier to the mobile charger. Hence, the following presents the *Request Threshold Lower Bound Constraint* which guarantees the sensor has enough energy for basic operations.

Recall that $E_i^{request}$ denotes the energy threshold. When the remaining energy of the sensor s_i is smaller than this threshold, it will send the recharging request to the *BS*. In case the sensor lately sends the recharging request to the *BS*, the mobile charger might not recharge the sensor in time. This can lead to a situation that the sensor switches to the sleep state, reducing the surveillance quality. Therefore, the $E_i^{request}$ should have a low bound. Let $E_i^{consume}$ denote the energy consumption rate of the sensor s_i. Let T_i^{wait} denote the waiting time of the sensor s_i for recharging, counting from the time point of sending the request. To guarantee the perpetual life of the sensor , the reserved waiting time should be larger than the time required for the movement of the diagonal of the monitoring area. It implies

$$T_i^{wait} > \sqrt{2} \times L_M / v. \quad (10)$$

To have enough remaining energy for energy consumption after sending the request, we have

$$\begin{aligned} E_i^{request} &> T_i^{wait} \times E_i^{consume} + E_i^{min} \\ &> \sqrt{2} \times L_M \times E_i^{consume} / v + E_i^{min}. \end{aligned} \quad (11)$$

Combining Exps. (10) and (11), the following presents the energy lower bound for the request threshold.

(2) *Request Threshold Lower Bound Constraint*

$$\sqrt{2} \times L_M \times E_i^{consume} / v + E_i^{min} < E_i^{request}. \quad (12)$$

In addition to the abovementioned two constraints, the battery capacity of the MC is another important constraint. The following further presents *Battery Low Bound Constraint*. Let E_{MC} denote the battery capacity of the *MC*. In a charing cycle T, the MC moves starting from the *BS*, charges the sensors, and then finally turns back to the *BS*. Let E_{MC}^{move} and L_{MC} denote the energy consumption rate of movement and the path length of the *MC*, respectively. Let E_{MC}^{move} denote the total energy required for the mobile charger moving length L_{MC}. The P_{MC}^{move} can be derived by

$$P_{MC}^{move} = E_{MC}^{move} \times L_{MC}. \quad (13)$$

In addition to the energy required for movement, the other energy consumption of the mobile charger is the energy for recharging the sensors. There is a loss of energy quantity when the MC charges the sensors. Let f_1 denote the energy conservation rate for charging the sensors. Let n_c denote the number of sensors the MC charged in a cycle T. Let $P_{MC}^{recharge}$ denote the total energy required for the MC to recharge the sensors in each cycle. The $P_{MC}^{recharge}$ can be derived by

$$P_{MC}^{recharge} = n_c \times (E - E_{min}) / f_1. \quad (14)$$

Hence, the total energy for the MC for moving length L_{MC} and recharging sensors in each cycle is $P_{MC}^{move} + P_{MC}^{recharge}$, which must be smaller than E_{MC}. The following *Battery Low Bound Constraint* reflects the abovementioned derivations.

(3) *Battery Low Bound Constraint*

$$E_{MC}^{move} \times L_{MC} + n_c \times (E - E_{min}) / f_1 < E_{MC}. \quad (15)$$

4 The Proposed CSCP Algorithm

Recall that a charging cycle T consists of two phases, namely the 'scheduling' and 'moving & recharging' phases. The proposed *CSCP* algorithm consists of 'initial', 'scheduling', and 'moving & recharging' procedures, which will be performed in the initial, scheduling, and moving & recharging phases, respectively. As shown in Figure 1, the initial phase aims to divide the monitoring area into some identical regular hexagon grids for simplifying the computations. Then each round has two phases, the scheduling and moving & recharging phases. In the scheduling phase, the major work of the MC is to choose a grid from the recharging request list. This grid will be the next charging target. Then, in the moving & recharging phase, the MC executes the moving & recharging procedure, moves to the scheduled grid (charging target), and then charges the sensors in that grid. The two procedures will be executed repeatedly until the energy of the MC is not enough to execute the charging task. Then the MC goes back to BS for power supplement.

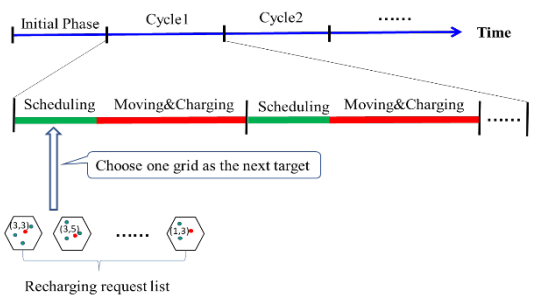

Figure. 1. Cycle T is made up of several rounds which consist of two tasks

The following presents the proposed algorithm.

4.1 Initial Phase

The goal of this phase is to divide the monitoring area M into some regular hexagonal grids. The reason for partitioning the area is illustrated below. The problem of constructing the optimal moving path for the MC is an NP problem that requires high computational complexity. To simplify the computational complexity, a regular hexagon grid is used as a basic grid to divide the monitoring area M. The size of the grid can affect the recharging performance. This issue will be discussed in the performance study section.

Let n_H denote the number of regular hexagon grids in M. As shown in Figure 2, the coordinates of the most top-left hexagon grid in M are set as (1,1). The x and y coordinates will be increased by one if the position of the hexagon grid shifts one position in the right or down direction, respectively. Let $H_{m,n}$ denote the hexagon grid with coordinates (m, n). Let $S_{m,n}$ denote the set of sensors in $H_{m,n}$. Let H_{center} denote the hexagon grid which contains the geometric center point of M. The BS is deployed at the center of H_{center}.

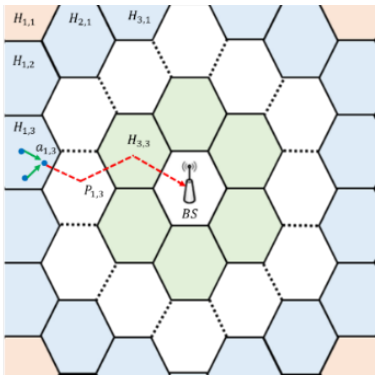

Figure 2. Grid-based monitoring area R

In each hexagon grid $H_{m,n}$, the sensors $s_i \in S_{m,n}$ form a cluster. Let $a_{m,n}$ denote the anchor of $H_{m,n}$, aiming to receive the sensing data from other sensors in $S_{m,n}$ and then forward them to BS. Initially, the sensor $s_i \in S_{m,n}$ closest to the center location of $H_{m,n}$ is chosen as $a_{m,n}$. All the sensors in each grid will act as anchors according to their remaining energy. This helps balance the remaining energy of sensors in each grid. When any sensor s_i in $H_{m,n}$ sends a recharging request, $H_{m,n}$ is added to the queue of the mobile charger.

4.2 Scheduling Phase

The purpose of this phase is to calculate the benefit of each grid, which is measured by the contribution to the surveillance quality. The following presents how to calculate the contribution of each grid. The MC will select the best grid which has the maximum benefit to the surveillance quality to be the next target grid.

The contribution of each grid is calculated based on its benefit for improving surveillance quality and the cost for MC to move to that grid. The location relation of point u and sensor s_i have two cases, depending on whether or not the point u falls into the sensing range r_s of sensor s_i. Assume that sensor s_i is the closest sensor to point u. Let $R_{i,u}$ denote the surveillance quality of point u. That is, the value

of $R_{i,u}$ represents the surveillance quality that the sensor s_i contributes to point u. In case that u falls in r_s, the sensing data of the sensor s_i can accurately represent the data of point u. Therefore, we have $R_{i,u} = 1$. On the contrary, in case that point u does not fall in r_s, using the collected data of the sensor s_i to represent the data of print u might not be accurate. Since the accuracy will be decreased with the distance between point u and the sensor s_i, the surveillance quality of point u will be measured by the following equation Eq. (16).

$$R_{i,u} = \begin{cases} 1 & d(s_i,u) \le r_s \\ (1-\rho)^{d(s_i,u)} & otherwise \end{cases}. \quad \textbf{(16)}$$

where $\rho \in (0,1)$ is a parameter to represent the reduction rate of the surveillance quality. Assume that point u falls in the grid $H_{m,n}$. Recall that $S_{m,n}$ denotes the set of sensors in the grid $H_{m,n}$. Next, the surveillance quality that all sensors $s_i \in S_{m,n}$ contribute to point u, denoted by $R^u_{m,n}$, can be further defined based on $R_{i,u}$. Herein, it is noticed that one sensor $s_i \in S_{m,n}$ can contribute the surveillance quality to point u at the time t only if the sensor s_i is working and is connected to the base station BS. This implies that $\lambda_{i,t} = 1$ and $\beta_{i,t} = 1$. The overall contribution of sensors in $S_{m,n}$ will be measured by the maximal contribution of data qualities contributed by sensors $s_i \in S_{m,n}$. Exp. (17) evaluates the value of $R^u_{m,n}$.

$$R^u_{m,n} = \max_{s_i \in S_{m,n}} \left(\lambda_{i,t} \times \beta_{i,t} \times R_{i,u}\right). \quad \textbf{(17)}$$

Till now, the surveillance quality of point u in the gird $H_{m,n}$ has been defined. The next step aims to define the surveillance quality of a grid $H_{m,n}$. Since a grid consists of an infinite number of points, the surveillance quality of the grid $H_{m,n}$ will be represented by the average quality of the randomly selected x points, denoted by $U_{m,n} = (u^1_{m,n}, u^2_{m,n}, \cdots, u^x_{m,n})$. The surveillance quality of any point, say u, in the gird $H_{m,n}$ is determined by the nearest sensor to u. Let $\mathcal{H}^{neighbor}_{m,n}$ denote the set of neighboring grids of $H_{m,n}$. Let $\mathcal{S}^{neighbor}_{m,n}$ denote the set of sensors in $\mathcal{H}^{neighbor}_{m,n}$. $\mathcal{H}^{neighbor+}_{m,n}$ denote the union of grids $H_{m,n}$ and $\mathcal{H}^{neighbor}_{m,n}$. Let $\mathcal{S}^{neighbor+}_{m,n}$ denote the set of sensors in $\mathcal{H}^{neighbor+}_{m,n}$. That is,

$$\mathcal{S}^{neighbor+}_{m,n} = \{s_i | s_i \in S_{m,n} \cup \mathcal{S}^{neighbor}_{m,n}\}. \quad \textbf{(18)}$$

Let $Q_{m,n}$, $\mathbb{Q}^{neighbor}_{m,n}$, $\mathbb{Q}^{neighbor+}_{m,n}$ denote the data qualities of grid $H_{m,n}$ and grid sets $\mathcal{H}^{neighbor}_{m,n}$ and $\mathcal{H}^{neighbor+}_{m,n}$, respectively.

As shown in Figure 3, if all sensors in $H_{m,n}$ stay in work state, the surveillance quality $\mathbb{Q}^{neighbor+}_{m,n}$ of $\mathcal{H}^{neighbor+}_{m,n}$ can be represented by the surveillance quality of sensors in $\mathcal{S}^{neighbor+}_{m,n}$. Similarly, if the sensors in $H_{m,n}$ stay in a sleep state, the surveillance quality $\mathbb{Q}^{neighbor}_{m,n}$ of $\mathcal{H}^{neighbor}_{m,n}$ can be represented by the surveillance quality of sensors in $\mathcal{S}^{neighbor}_{m,n}$. The $\mathbb{Q}^{neighbor}_{m,n}$ and $\mathbb{Q}^{neighbor+}_{m,n}$ can be obtained by applying Eqs. (19) and (20), respectively.

$$\mathbb{Q}^{neighbor}_{m,n} = \sum_{1 \le j \le x} \max_{s_i \in \mathcal{S}^{neighbor}_{m,n}} \left(R_{i,u^j_{m,n}}\right). \quad \textbf{(19)}$$

$$\mathbb{Q}^{neighbor+}_{m,n} = \sum_{1 \le j \le x} \max_{s_i \in \mathcal{S}^{neighbor+}_{m,n}} \left(R_{i,u^j_{m,n}}\right). \quad \textbf{(20)}$$

The surveillance quality $Q_{m,n}$ contributed by $H_{m,n}$ at time t can be obtained by applying Eq. (21).

$$Q^t_{m,n} = \mathbb{Q}^{neighbor+}_{m,n} - \mathbb{Q}^{neighbor}_{m,n}. \quad \textbf{(21)}$$

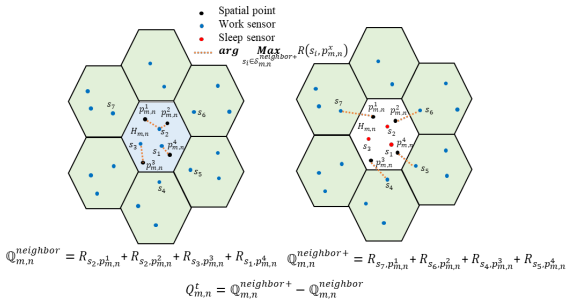

Figure 3. Representative of the sensor

In addition to the surveillance quality contribution of each grid, the network connectivity contribution is another crucial parameter that should be taken into account as the MC makes a charging schedule. The sensing data of sensors in $H_{m,n}$ are transmitted along a path, denoted by $P_{m,n}$, from $a_{m,n}$ to BS. As shown in Figure 2, the hexagon grid $H_{3,3}$ is on the path $P_{1,3}$ and is closer to the BS than $H_{1,3}$, the failure of $s_k \in S_{3,3}$ might block the routing path. This implies that $H_{3,3}$ has a larger contribution than $H_{1,3}$ in considering the network connectivity. Therefore, the hexagon grids near the BS should have a larger contribution than the far-away hexagon grids. The sensors in the hexagon grid closer to the BS should be preferentially charged to prevent network disconnection.

Let $\mathcal{H}^{connnect}_{m,n}$ denote the set of hexagon grids that the path from any grid, say $H_{i,j}$, in $\mathcal{H}^{connnect}_{m,n}$ to BS will pass through $H_{m,n}$. Let $Q^{connect}_{m,n}$ denote the *connectivity benefit* of hexagon grid $H_{m,n}$ at time t, which can be calculated by applying Eq. (22).

$$Q_{m,n}^{t,connect} = \sum_{H_{i,j} \in \mathcal{H}_{m,n}^{connnect}} Q_{i,j}^{t}. \quad (22)$$

Let $B_{m,n}$ denote the recharging benefit of $H_{m,n}$ at time t, which can be calculated by applying Eq. (23).

$$B_{m,n} = Q_{m,n}^{t} + Q_{m,n}^{t,connect}. \quad (23)$$

Let Ω denote the request recharging queue of MC. The function of this queue is to manage the recharging requests sent from anchors. Each request message is stored in the request queue Ω which contains the following information

$$r_{i,j} = \left(H_{i,j}, t_{sent}, \left\{(s_k, E_k) | s_k \in S_{i,j}\right\}\right)$$

where t_{sent} denotes the sending time of the recharging request message and (s_k, E_k) denotes the pair of sensor s_k and its remaining energy at the time t_{sent}.

The MC will consider each grid $H_{i,j}$ in the request queue Ω and calculate the benefit $B_{i,j}$ to decide whether or not $H_{i,j}$ is the next target grid for recharging. However, in addition to the benefit calculation, the cost of passing the grid $H_{i,j}$ should be considered. The following describes how the MC calculates the cost for each grid $H_{i,j}$ in Ω.

The major cost of visiting the grid $H_{m,n}$ consists of two parts: the movement and the recharging costs. These costs can be measured in terms of time. Let $t_{m,n}^{travel}$ denote the travel time required for the MC moving from the current position to the grid $H_{m,n}$. Let $t_{m,n}^{charge}$ denote the predicted time required for the MC recharging of the sensors in $H_{m,n}$. The prediction of $t_{m,n}^{charge}$ can be achieved by considering the remaining energy of each sensor in $H_{m,n}$. Recall that $E_{i,t}^{rem}$ denote the remaining energy of the sensor $s_i \in S_{m,n}$. The prediction charging time $t_{m,n}^{charge}$ of grid $H_{m,n}$ can be measured by:

$$t_{m,n}^{charge} = \sum_{s_i \in S_{m,n}} \left(E - E_{i,t}^{rem}\right) / P_{s_i}. \quad (24)$$

Let $t_{m,n}$ denote the total cost of the grid $H_{m,n}$. The value of $t_{m,n}$ can be calculated by applying Eq. (25).

$$t_{m,n} = t_{m,n}^{travel} + t_{m,n}^{charge}. \quad (25)$$

Let $REI_{m,n}$ denote the *Recharging Efficiency Index* which is the obtained benefit divided by the cost. That is,

$$REI_{m,n} = B_{m,n} / t_{m,n}. \quad (26)$$

The charging strategy is to consider the grid where some sensors have low remaining energy and the grid's *REI* is the largest. That is, the MC will recharge the hexagon grid H^{best} if it satisfies Eq. (27).

$$H^{best} = arg \max_{H_{m,n} \in \Omega} REI_{m,n}. \quad (27)$$

Till now, the MC has determined the next recharging grid. This decision is made by taking into consideration the benefit of surveillance quality, connectivity, and the cost of each requested grid. The next step is to recharge the grid, which will be discussed in the next subsection.

4.3 Moving & Recharging Phase

This sub-section aims to construct a path along which the MC moves and recharges the sensors in the target grid $H_{m,n}$. Herein, it is noticed that any sensor falling in the charging range of MC can be recharged wirelessly. To ensure that each sensor can be fully recharged, the *Full Recharged Range* property, denoted by FR^2, is proposed as follows.

Recall that r_{MC} denote the charging radius of MC. Consider the scenario depicted in Figure 4. The blue circle R_i denotes the recharging range of the sensor s_i, which is constructed by charging radius r_{MC} using the location of the sensor s_i as the central point. Let line L be a moving path of MC, which passes through R_i starting at a time point t_1 and ending at the time point t_2. Let R_i^{full} denote the fully recharging circle which satisfies the following condition.

$$\int_{t_1}^{t_2} P_{s_i} dt \geq E - E_{i,t_1}^{rem} - \sum_{t_j=t_1}^{t_2} \left(E_{i,j}^{s} + E_{i,j}^{R} + E_{i,j}^{T}\right). \quad (28)$$

Figure 4 depicts the fully recharging circle R_i^{full} which is a dotted blue circle tangent to the line L.

Full Recharged Range* (FR^2) *Property:

The sensor s_i can be full recharged if the recharging path and the circle R_i^{full} intersect at least one point.

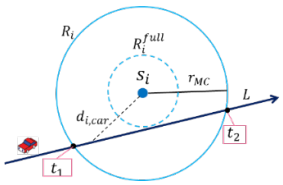

Figure 4. Representative of the sensor

Proof:

Let P_{s_i} be the received energy of the sensor s_i. The received energy mainly depends on the distance between the MC and the sensor s_i and can be measured by Exp. (7). To guarantee that the sensor s_i can be fully recharged, the received energy should be larger than or equal to the consumed energy of the sensor s_i. Since the sensor s_i falls in the charging range of the MC from time t_1 to t_2, the total received energy of the sensor s_i from the MC can be derived by:

$$\int_{t_1}^{t_2} P_{s_i} dt. \tag{29}$$

The consumed energy can be calculated by the total energy minus the remaining energy. At time t_1, the remaining energy is E_{i,t_1}^{rem}. However, the sensor s_i continuously consumes energy. Let E_{t_1,t_2}^{loss} denote the energy loss from time t_1 to t_2. The E_{t_1,t_2}^{loss} can be derived by:

$$E_{t_1,t_2}^{loss} = \sum_{t_j=t_1}^{t_2} \left(E_{i,j}^{s} + E_{i,j}^{R} + E_{i,j}^{T} \right). \tag{30}$$

As a result, the total consumed energy of the sensor s_i is:

$$\begin{aligned} E_{i,t_2}^{rem} &= E - E_{i,t_1}^{rem} - E_{t_1,t_2}^{loss} \\ &= E - E_{i,t_1}^{rem} - \sum_{t_j=t_1}^{t_2} \left(E_{i,j}^{s} + E_{i,j}^{R} + E_{i,j}^{T} \right). \end{aligned} \tag{31}$$

Therefore it is proved that the sensor s_i can be fully recharged if the following Exp. (32) holds.

$$\int_{t_1}^{t_2} P_{s_i} dt \geq E - E_{i,t_1}^{rem} - \sum_{t_j=t_1}^{t_2} \left(E_{i,j}^{s} + E_{i,j}^{R} + E_{i,j}^{T} \right). \tag{32}$$

The abovementioned FR^2 theorem will be applied to develop the charging path for the MC to satisfy the recharging requests of all sensors in $H_{m,n}$. The following presents the path construction algorithm. The algorithm mainly consists of the initial path construction phase, virtual sensor replacement phase, and FR^2 path reconstruction phase. The first phase aims to construct an initial path that passes through all sensors. According to this path, the MC can be aware order of each visited sensor and the trend of the shortest path. The second and third phases aim to further reduce the path length such that the movement cost can be reduced, improving the recharging efficiency. More specifically, the virtual sensor replacement phase aims to reduce the path length by using one virtual sensor to replace some sensors whose FR^2 are overlapped with each other. The third phase mainly applies the FR^2 theorem to further reduce the path length. In the following, the details of the three phases will be presented.

Phase I: Initial Path Construction Phase

This phase aims to construct an initial charging path that passes through all sensors in H_{mn}. Let $|S_{m,n}|$ denote the number of sensors in H_{mn}. Let $P^I = (s_0, s_1, ..., s_{|Sm,n|})$ denote the initial path which can be easily constructed by applying the existing XT algorithm [21]. As shown in Figure 5, the initial path $P^I = (s_0, s_1, s_4, s_5, s_6, s_7, s_8, s_9)$, which is marked with a black dashed line, is constructed.

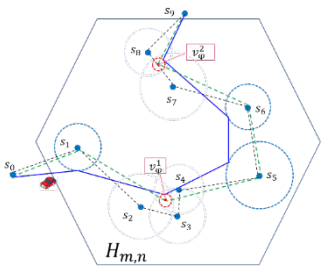

Figure 5. Charging path in the $H_{m,n}$

Phase II. Virtual Sensor Replacement Phase.

This phase aims to reduce the length of the initial path constructed in Phase I. Let $S^{overlap}$ be the *Completed Overlapped Sensor Set* which is a collection of the sensors that the FR^2 of each sensor in $S^{overlap}$ should overlap with the FR^2 of all the other sensors in $S^{overlap}$. That is,

$$\begin{aligned} S^{overlap} = \{ & s_i^{overlap} | s_i^{overlap}.FR^2 \cap s_j^{overlap}.FR^2 \\ & \neq \varnothing, \forall s_j^{overlap} \in S^{overlap} \}. \end{aligned} \tag{33}$$

Let φ denote the largest inscribed circle inside the overlapped FR^2 of all sensors in $S^{overlap}$. Let v_φ denote the center point of φ. Let P^{II} denote the new path where all sensors $s_i^{overlap} \in S^{overlap}$ are replaced by v_φ in the original path P^I. As shown in Figure 6, since the new path P^{II} intersects with the FR^2 of each sensor $s_i^{overlap} \in S^{overlap}$ at least two points, each sensor $s_i^{overlap} \in S^{overlap}$ can be fully recharged according to the *Full Recharged Range Property*.

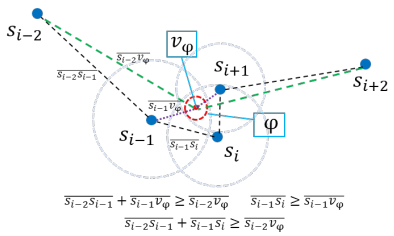

Figure 6. Virtual sensor replacement

Hence, the MC moves along the path P^{II} to charge the sensors, the length of the charging path will be reduced.

Phase III. Path Reduced Phase

This phase aims to further reduce the length of the path P^{II} constructed in Phase II. Consider the *Full Recharged Range Property*, the charging path P^{II} only needs to have an intersection point with the FR^2 of the sensor s_i. It guarantees that the sensor s_i can be fully recharged. Herein, it is noticed that the *Full Recharged Range Property* can be applied to three sensors. The first and the third sensors are the starting and end sensors, while the second one is recharged sensor.

Initially, three successive sensors s_0, s_1, s_2 in the path P^{II} is collected, let P_1 denote their paths of them,

$$P_1 = \{s_0, s_1, s_2\}. \tag{34}$$

The following will introduce the *basic path reduction operation*. Let $\overline{s_0 s_2}$ denote the line segment connecting s_0 and s_2. As shown in Figure 7(a), if $\overline{s_0 s_2}$ intersects with the FR^2 of s_1, then the intersection point closer to s_2, called $\hat{s}_1$, will replace s_1 to form a new path. Otherwise, as shown in Figure 7(b), line $\overline{s_0 s_2}$ does not intersect with the FR^2 of s_1. In this case, moving line $\overline{s_0 s_2}$ closer to s_1 until it intersects with the FR^2 of s_1 at point $\hat{s}_1$. Then a new path will be created by replacing the point s_1 with point $\hat{s}_1$.

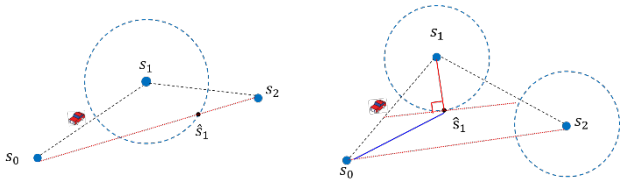

(a) Case 1: edge $\overline{s_0 s_2}$ and FR^2 of s_1 have intersection point

(b) Case 1: edge $\overline{s_0 s_2}$ and FR^2 of s_1 have no intersection point

Figure 7. Representative of the sensor

Similarly, assume that $P_i = \{\hat{s}_{i-1}, s_i, s_{i+1}\}$ has been applied the abovementioned *basic path reduction operation* which has reduced the path length of the subpath or original P_i. Then the next step is to apply *the basic path reduction operation* on the next subpath $P_{i+1} = \{\hat{s}_i, s_{i+1}, s_{i+2}\}$, aiming to reduce the path length of the subpath of P_{i+1}. The *basic path reduction operation* will be repeatedly applied on the next subpath until all possible subpath has been applied.

Let P^{III} denote the final charging path. Then the path P^{III} can be obtained by

$$P^{III} = (s_0, \ldots, \hat{s}_{i-1}, \hat{s}_i, \hat{s}_{i+1}, \ldots, s_{|P^{III}|}). \quad (35)$$

Hence the *MC* moves to charge the sensors along P^{III}, the length of the charging path will be reduced.

The total time cost for recharging all sensors in $H_{m,n}$ can be calculated by applying Eq. (36).

$$t_{m,n} = |P^{III}| / v. \quad (36)$$

Recall that the $REI_{m,n}$ denotes the *Recharging Efficiency Index* which can be obtained by Exp. (26).

$$REI_{m,n} = B_{m,n} / t_{m,n}.$$

Figure 8 summarizes the algorithm proposed in this section. In step 1, the monitoring area M is divided into n_M regular hexagonal grids, aiming to simplify the computational complexity. Step 2 further defines $H_{m,n}$ and $S_{m,n}$. Step 3 checks if the request recharging queue Ω is empty. If it is not the case, step 4 will be applied. Otherwise, the mobile charger will wait for the new charging request. Step 4 calculates the surveillance quality by applying Exp. (21). In step 5, the connectivity benefit of each hexagon grid in Ω is calculated. In step 6, the recharging benefit of each hexagon grid in Ω is calculated. In step 7, the distance costs to recharge each hexagon grid are measured by the travel time required for the *MC* moving from the current position to the grid, plus the predicted time required for the *MC* recharging the sensors. In step 8, the *Recharging Efficiency Index* of each hexagon grid in Ω is calculated. In step 9, the *MC* selects the grid H^{best} which has the maximal *REI* as the next target to charge. In step 10, the *MC* constructs an initial charging path P^I that passes through all sensors in H^{best}. Step 11 adopts the *Virtual Sensor Replacement* to construct P^{II} aiming to reduce the length of the path P^I. Step 12 applies the *Full Recharged Range Property* to construct the charging path P^{III}.

Algorithm: *CSCP*	
Inputs: The location of each sensor s_i, the size of the monitoring area, and the grid length.	
Output: The recharging path of the mobile charger.	
	/* *Initialization Phase* */
1	Partition the M into n_M regular hexagonal grids
2	Let $S_{m,n}$ denote the set of sensors in $H_{m,n}$
3	While $\Omega \neq \emptyset$
	/* *Scheduling Phase**/
	/* Calculate the surveillance quality of $H_{m,n} \in \Omega$ */
4	$Q^t_{m,n} = \sum_{1 \le j \le x} \max_{s_i \in S^{neighbor}_{m,n}} (R_{i,u^j_{m,n}}) - \sum_{1 \le j \le x} \max_{s_i \in S^{neighbor}_{m,n}} (R_{i,u^j_{m,n}})$
	/* Calculate the connectivity of $H_{m,n}$ */
5	$Q^{t,connect}_{m,n} = \sum_{H_{i,j} \in \chi^{connect}_{m,n}} Q^t_{i,j}$
	/* Calculate the benefit of $H_{m,n}$ */
6	$B_{m,n} = Q^t_{m,n} + Q^{t,connect}_{m,n}$
	/* The total cost to charge $H_{m,n}$ */
7	$t_{m,n} = t^{travel}_{m,n} + t^{charge}_{m,n}$
	/* The *Recharging Efficiency Index* of $H_{m,n}$ */
8	$REI_{m,n} = B_{m,n} / t_{m,n}$
	/* Select the grid that has the maximal *REI* to be recharged */
9	$H^{best} = \arg\max_{H_{m,n}} REI_{m,n}$
	/* *Moving & Recharging Phase* */
	/* Initial Path Construction Task */
10	Construct an initial charging path P^I in H_{mn} that passes through all sensors by the XT algorithm: $P^I = (s_0, s_1, \cdots, s_n)$
	/* Virtual Sensor Replacement Task */
11	Reduce the length of P^I by the *Virtual Sensor Replacement*: $P^{II} = (s_0, \cdots, v^k_\varphi, \cdots, s_n)$
	/* Path Reduced Task */
12	Reduce the length of P^{II} by the *Full Recharged Range Property*: $P^{III} = (s_0, \hat{s}_1, \hat{s}_2, \cdots, \hat{s}_{n-1}, s_n)$
13	Until completing the monitoring task

Figure 8. Pseudocode of the proposed *CSCP*

According to the proposed *CSCP* algorithm, the *MC* can charge the sensors with a high charging efficiency. As a result, the monitor area can keep up a good surveillance quality at any time t. This policy helps achieve the goal given in Eq. (6). The following illustrates the computational complexity analysis of the proposed *CSCP* algorithm and compares it with the complexities of [11] and [15].

The computational complexity of the proposed algorithm is analyzed as follows. In steps 1-2, the dividing of the whole monitor area requires $O(n_H)$. In step 4, the computation of surveillance quality of any point $u_{m,n}^j$ requires $O(n_M/n_H)$. Since the calculation of the surveillance quality needs to take x samples of $H_{m,n}$, it requires $O(x \times n_M/n_H)$. In step 5, the connectivity contribution of a grid is determined by the number of grids passing through this grid to the BS. The total number of grids in the monitoring area is n_H. Therefore, the forwarding load of each grid is at most n_H-1. This also indicates that there are at most $n_H - 1$ grids connected to a certain grid. As a result, the computation cost is $(n_H - 1)$. The computational complexity of step 5 is $O(n_H)$. In steps 6-8, the computational complexity is $O(1)$. In step 9, the grid with the largest *REI* will be selected to be recharged. Since the number of candidates is at most n_H grids, it requires $O(n_H)$. In step 10, the construction of the initial charging path requires $O((n_M/n_H)^2)$. In step 11, a recursive algorithm is used to derive $S^{overlap}$ in each grid. This requires $O(log(n_M/n_H))$. Then, the virtual sensor is used to replace the $S^{overlap}$, aiming to reduce the path length. This requires $O(1)$. Therefore, the total computational complexity of step 11 is $O(log(n_M/n_H))$. In step 12, the *basic path reduction operation* is used to reduce the path length. This requires $O(n_M/n_H - 2)$. In general, the number of sensors is far greater than that of the grids. Therefore, the computational complexity of each While loop is $O(n_H) + O(x \times n_M/n_H) + O((n_M/n_H)^2)$ which can be simplified as $O((n_M/n_H)^2)$. Assume that each hexagon grid is charged once, and the number of the loops is n_H. Finally, the total complexity of the proposed *CSCP* algorithm is $O(n_M^2/n_H)$. The total complexities of the references [11] and [15] are $O(n_M^2)$ under the same condition.

5 Simulation

This section makes inquiries about the performance improvement of the proposed CSCP algorithm against the existing studies YCC [11] and ERSQ [15]. The parameters used in the experiments are given in Table 2. The setting values of these parameters mainly refer to studies [19-20].

Table 2. Simulation parameters

Parameters	Values
Monitoring area	100m*100m
Number of sensors	100-200
Node deployment	Randomly
The grid length	5m-20m
The sensing range: r_s	5m
The reduction rate of the surveillance quality: ρ	0.9
Mobile charger speed: v	5 m/s
The energy consumption of movement for the mobile charger: E_{move}	30 J/m
The required energy for sensing: E_s	0.05J
The required energies for receiving and transmitting: E_T, E_R	0.02J
The transmitted power of the mobile charger: P_{car}	5 J/s
The initial energy of each sensor: E	1000 J

In Figure 9, the monitoring area is divided into 52 grids. All sensors are assumed to be randomly deployed. The sensors in the same and neighboring grids can communicate with each other. Figure 9 indicates a deployment snapshot of 200 sensor nodes in the area. To calculate the surveillance quality of each grid, the proposed CSCP randomly selects 6 points, calculates their surveillance qualities, and finally takes the total surveillance quality of the six selected points as the surveillance quality of this grid.

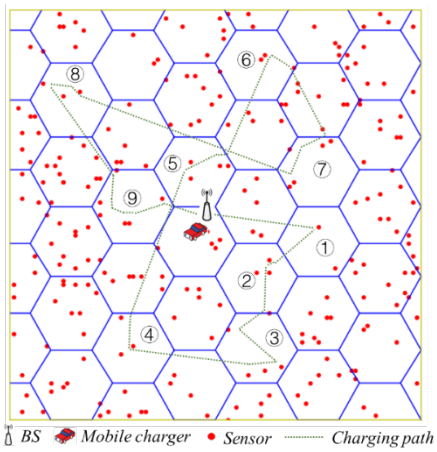

Figure 9. Simulation environment

In Figure 10, the three algorithms are compared in surveillance quality. The number of sensors is varied ranging from 100 to 200. The number of elapsed cycles varies from 5 to 25. The grid length is set at 10 meters. A common trend of the three algorithms is that their surveillance qualities are increased with the number of deployed sensors but decreased with the elapsed time. The density is increased with the number of deployed sensors, which helps improve its contribution to surveillance quality. As a result, the surveillance qualities of the three algorithms increase with the number of deployed sensors. In addition, the sensors keep working, which consumes energy. Since the remaining energy of each sensor is reduced with the elapsed time, the network connectivity is reduced. The proposed *CSCP* has better performance than the compared related studies. The reason is that the proposed *CSCP* algorithm further considers the surveillance quality and priors to recharge the grid which has the largest improvement in terms of surveillance quality.

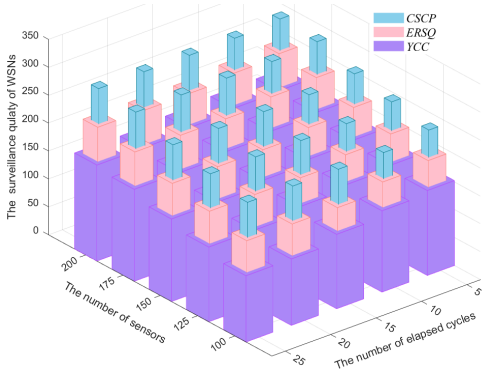

Figure 10. Comparison of three algorithms in terms of surveillance quality of the monitoring area

Figure 11 compares the three algorithms in the number of working sensors. Herein, a working sensor means that it stays in a sensing state and the *BS* can successfully receive its sensing data. In some cases, although a sensor is working, it will not be taken into account of a working sensor. The key reason is that the sensing data are unable to be forwarded to the *BS* because the network is disconnected. Two common trends of the compared algorithms are found. First, the number of working sensors grows with the number of deployed sensors. Second, the number of working sensors decreases when the elapsed time grows. The main reason is that each working sensor consumes its energy for executing sensing and data forwarding operations. As a result, some sensors with heavy forwarding loads will stay in the sleep state. Therefore, the number of working sensors decreases when the elapsed time grows.

The proposed *CSCP* algorithm has a larger number of working sensors than the other two algorithms in all cases. The main reason is that the existing *YCC* algorithm only takes into account the remaining energy and the distance. In comparison, the proposed *CSCP* further takes into account the surveillance quality and network connectivity. In some cases, the *YCC* might go to recharge one sensor which lacks connectivity to the base station. However, the proposed *CSCP* will not recharge the sensor since it cannot contribute to the surveillance quality. On the other hand, the *ERSQ* algorithm considered network connectivity and path length. However, the *MC* did not construct a path to recharge all sensors in one grid. Instead, it stopped at the center location of the grid and recharged all sensors, which requires much time when recharging the sensors. In comparison, the proposed *CSCP* constructs an efficient path for recharging all sensors in one grid, saving much time for recharging. This helps the *MC* recharge more grids, increasing the number of working sensors.

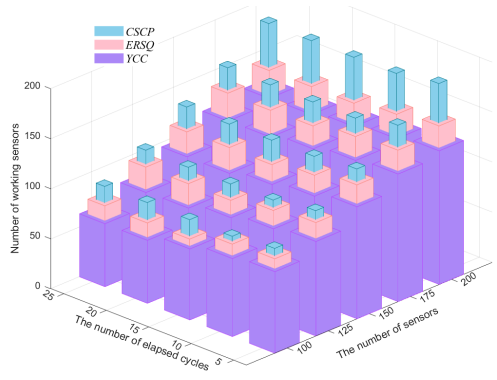

Figure 11. Comparison of three algorithms in terms of the number of working sensors

Figure 12 compares the surveillance qualities of the three algorithms. The number of sensors is changed ranging from 100 to 200. The grid length is controlled from 5 to 20 meters. The number of elapsed cycles is set at 10. To calculate the surveillance quality, there are 312 points randomly chosen in the monitor area. The three algorithms have a similar trend that the surveillance quality of WRSN increases when the number of deployed sensors grows. The key reason is that network connectivity has a significant impact on surveillance quality. The other trend is that the surveillance quality is decreased when the hexagon edge is smaller. The reason is that each sensor needs to consume more energy for forwarding data to the sensor which is located in the neighboring grid. As a result, the sensors switch to the sleep state early, reducing the surveillance quality. In summary, the proposed *CSCP* algorithm achieves better performance than the other two algorithms. The reasons are similar since the proposed *CSCP* takes connectivity into account.

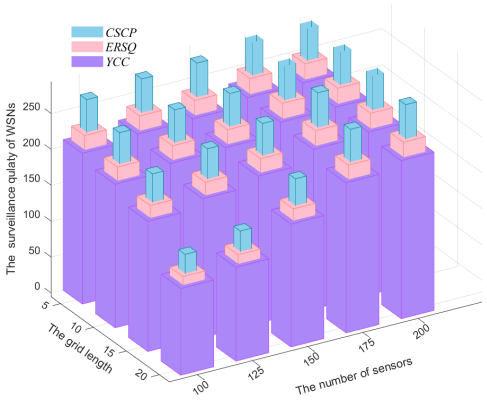

Figure 12. Comparison of three algorithms in terms of the surveillance quality of the monitoring area

Figure 13 compares the three algorithms in terms of the number of working sensors. The observation time is ranging from 5 to 25 cycles. The grid length is controlled from 5 to 20. The number of sensors is set at 100. Three algorithms have a common trend that the number of working sensors decreases with both the elapsed time and the length of the hexagon edge. This occurs because a larger length of the hexagon edge increases the energy consumption of data forwarding. As a result, sensors get into the sleep state early, which reduces the number of working sensors. In addition, applying the proposed *CSCP*, the number of working sensors is stable after 10 cycles. However, the other two existing mechanisms require more cycles to achieve a stable number of working sensors. The major reason is that the *CSCP* recharges more sensors than the other as compared to *YCC* and *ERSQ* within a fixed time.

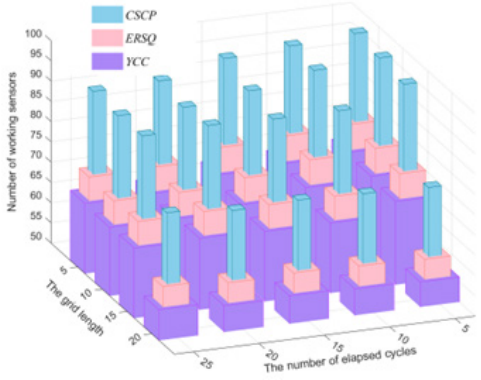

Figure 13. Comparison of three algorithms in terms of the number of working sensors

Figure 14 further compares the three algorithms in terms of the recharging efficiencies which is defined as the number of recharged sensors connected to the *BS* divided by the charging time of the *MC* . The number of sensors is changed from 100 to 200 while the grid length is changed from 5 to 20 meters. The number of elapsed cycles is set at 10. In comparison, the proposed *CSCP* algorithm has a better performance than the other two algorithms. The key reason is that the proposed *CSCP* algorithm further takes into account the recharging cost and the network connectivity contribution.

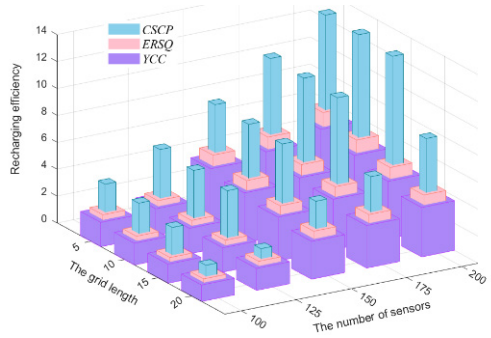

Figure 14. Comparison of three algorithms in terms of the recharging efficiency

Figure 15 investigates the improvement of the proposed algorithm in the effectiveness index of working sensors. The effectiveness index of working sensors is defined as the ratio of the number of working sensors to the number of sensors in a working state. The number of sensors is controlled from 100 to 200 and the grid length is set at 10 meters. The number of elapsed cycles is set at 10. The compared algorithms have a common trend that the effectiveness indices of the working sensors are increased with the number of sensors. The reason is that there are more sensors in each hexagonal grid, which improves the surveillance quality of the grid. In summary, the proposed *CSCP* algorithm achieves better performance than the other algorithms because it further considers the recharging cost as well as the connectivity contribution.

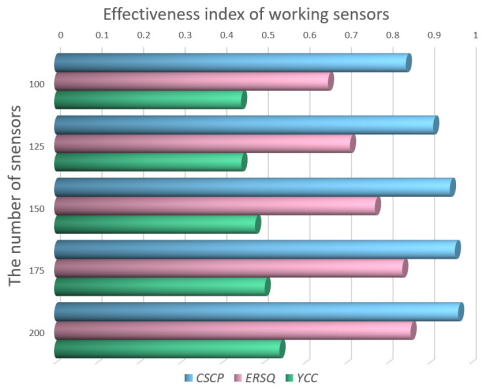

Figure 15. Comparison of three algorithms in terms of the effectiveness index of working sensors

6 Conclusion

This paper proposes a *CSCP* algorithm aiming to maximize the surveillance quality of a given WRSN. Unlike the existing studies, this paper additionally takes into account the surveillance quality and network connectivity benefits, and prior to recharging those sensors which contribute significant surveillance quality and/or connectivity contributions. The proposed *CSCP* algorithm is composed of three phases. The *Initial Phase* divides the surveillance area into equal-sized grids and constructs a coordinate system. Then the *scheduling phase* further determines the next recharging grid by considering benefits including the surveillance quality and connectivity contributions and the cost of each requested grid. Finally, the *moving & recharging phase* constructs a path from the current position to the target grid along which the *MC* moves and recharges the sensors in the target grid. The performance study reveals that the proposed *CSCP* algorithm has better performance than the existing algorithms in terms of surveillance quality and recharging efficiency in all cases. Future work will consider the cooperation of multiple mobile chargers to improve the surveillance quality of the monitoring area.

References

[1] H. Yiğitler, O. Kaltiokallio, R. Hostettler, A. S. Abrar, R. Jäntti, N. Patwari, S. Särkkä, RSS models for respiration rate monitoring, *IEEE Transactions on Mobile Computing*, Vol. 19, No. 3, pp. 680-696, March, 2020.

[2] S. Wu, H. Dai, L. Xu, L. Liu, F. Xiao, J. Xu, Comprehensive cost optimization for charger deployment in multi-hop wireless charging, *IEEE Transactions on Mobile Computing*, Vol. 1, No. 1, pp. 1-1, March, 2022.

[3] Y. Chen, Y. Jie, J. Zhu, Q. Lu, Y. Cheng, X. Cao, Z. L. Wang, Hybridized triboelectric-electromagnetic nanogenerators and solar cell for energy harvesting and wireless power transmission, *Nano Research*, Vol. 15, No. 3, pp. 2069-2076, March, 2022.

[4] A. Prasanna, V. Kumar, S. Dhok, Cooperative Communication and Energy-Harvesting-Enabled Energy-Efficient Design of MI-Based Clustered Nonconventional WSNs, *IEEE Systems Journal*, Vol. 14, No. 2, pp. 2293-2302, June, 2020.

[5] T. Zhao, L. Wang, K. Chin, C. Yang, Routing in Energy Harvesting Wireless Sensor Networks With Dual Alternative Batteries, *IEEE Systems Journal*, Vol. 15, No. 3, pp. 3970-3979, September, 2021.

[6] H. Azarhava, J. M. Niya, Energy efficient resource allocation in wireless energy harvesting sensor networks, *IEEE Wireless Communications Letters*, Vol. 9, No. 7, pp. 1000-1003, July, 2020.

[7] A. Kurs1, A. Karalis, R. Moffatt1, J. Joannopoulos, P. Fisher, M. Soljačić, Wireless power transfer via strongly coupled magnetic resonances, *Science*, Vol. 317, No. 5834, pp. 83-84, July 2007.

[8] A. Kurs, R. Moffatt, M. Soljačić, Simultaneous mid-

range power transfer to multiple devices, *Applied Physics Letters*, Vol. 96, No. 4, Article No. 44102, January, 2010.
[9] X. Tian, K. T. Chau, W. Liu, H. Pang, C. H. T. Lee, Maximum power tracking for magnetic field editing-based omnidirectional wireless power transfer, *IEEE Transactions on Power Electronics*, Vol. 37, No. 10, pp. 12901-12912, October, 2022.
[10] K. Dautov, M. S. Hashmi, N. Nasimuddin, M. A. Chaudhary, G. Nauryzbayev, Quantifying the impact of slow wave factor on closed-loop defect-based WTP systems, *IEEE Transactions on Instrumentation and Measurement*, Vol. 71, pp. 1-10, June, 2022.
[11] H. Yu, G. Chen, S. Zhao, C. Chang, Y. Chin, An efficient wireless recharging mechanism for achieving perpetual lifetime of wireless sensor networks, *Sensors*, Vol. 17, No. 1, Article No. 13, January, 2017.
[12] W. Xu, W. Liang, X. Jia, H. Kan, Y. Xu, X. Zhang, Minimizing the maximum charging delay of multiple mobile chargers under the multi-node energy charging scheme, *IEEE Transactions on Mobile Computing*, Vol. 20, No. 5, pp. 1846-1861, May, 2021.
[13] C. Sha, Y. Sun, R. Malekian, Research on cost-balanced mobile energy replenishment strategy for wireless rechargeable sensor networks, *IEEE Transactions on Vehicular Technology*, Vol. 69, No. 3, pp. 3135-3150, March, 2020.
[14] B. Dande, S. Y. Chen, H. C. Keh, S. J. Yang, D. S. Roy, Coverage-aware recharging scheduling using mobile charger in wireless sensor networks, *IEEE Access*, Vol. 9, pp. 87318-87331, June, 2021.
[15] Y. Kan, C. Y. Chang, C. H. Kuo, D. S. Roy, Coverage and Connectivity aware energy charging mechanism using mobile charger for WRSNs, *IEEE Systems Journal*, Vol. 16, No. 3, pp. 3993-4004, September, 2022.
[16] X. Yang, G. Han, L. Liu, A. Qian, W. Zhang, IGRC: An improved grid-based joint routing and charging algorithm for wireless rechargeable sensor networks, *Future Generation Computer Systems*, Vol. 92, pp. 837-845, March, 2019.
[17] A. Tomar, K. Nitesh, P. K. Jana, An efficient scheme for trajectory design of mobile chargers in wireless sensor networks, *Wireless Networks*, Vol. 26, No. 2, pp. 897-912, February, 2020.
[18] C. Lee, W. Na, G. Jang, C. Lee, S. Cho, Energy-efficient and delay-minimizing charging method with a multiple directional mobile charger, *IEEE Internet of Things Journal*, Vol. 8, No. 10, pp. 8291-8303, May, 2021.
[19] C. Wang, J. Li, Y. Yang, F. Ye, A Hybrid Framework Combining solar energy harvesting and wireless charging for wireless sensor networks, *IEEE INFOCOM 2016 - The 35th Annual IEEE International Conference on Computer Communications*, San Francisco, CA, USA, 2016, pp. 1-9.
[20] W. Tu, X. Xu, T. Ye, Z. Cheng, A Study on Wireless Charging for Prolonging the Lifetime of Wireless Sensor Networks, *Sensors*, Vol. 17, No. 7, Article No. 1560, July, 2017.
[21] X. Bresson, T. Laurent, The transformer network for the traveling salesman problem, March, 2021, https://arxiv.org/abs/2103.03012.

Biographies

Yuanping Kan received the M.S. degree from Wuhan University of Technology, China, in 2006. He received the Ph.D. degree from Tamkang University, Taiwan, in 2022. He is currently a Full Lecturer at Fujian Polytechnic Normal University, China. His current research interests are Information Security, Wireless Sensor Networks, and Artificial Intelligence.

Chih-Yung Chang (M'05) received the Ph.D. degree from the National Central University, Taiwan, in 1995. He is currently a Full Professor at Tamkang University, Taiwan. His current research interests include IoT, WSNs, artificial intelligence and deep learning. He has served as an Associate Guest Editor for several SCI-indexed journals.

Shih-Jung Wu is a Professor and the Dean of Student Affairs at the Tamkang University, Taiwan. He received M.S. and Ph.D. degrees from Tamkang University, Taiwan, in 2001 and 2006, respectively. His current research interests include Parallel Computing, Data Mining, Wireless Networks, and Artificial Intelligence.

Chin-Hwa Kuo received the Ph.D. degree from the University of Notre Dame, USA, in 1994. Currently, he is a full professor and Chief of Information Officer at Tamkang University, Taiwan. His research interests include multimedia processing and applications, learning analytics, and large scale deployment of ICT in education.

Diptendu Sinha Roy received the Ph.D. degree from Birla Institute of Technology, India in 2010. In 2016, he joined the National Institute of Technology (NIT) Meghalaya, India as an Associate Professor. His current research interests include software reliability, Distributed and Cloud Computing and IoT, Artificial Intelligence and Machine Learning.